

## First-principles calculations on structural stability and electronic properties of nitrogen-doped lutetium hydrides under pressure

Xiaokuan Hao,<sup>1</sup> Xudong Wei,<sup>1</sup> Hanyu Liu,<sup>2,3</sup> Xiaoxu Song<sup>1</sup>, Rongxin Sun,<sup>1</sup> Guoying Gao<sup>1,\*</sup> and Yongjun Tian<sup>1</sup>

<sup>1</sup>Center for High Pressure Science (CHiPS), State Key Laboratory of Metastable Materials Science and Technology, Yanshan University, Qinhuangdao, Hebei 066004, China

<sup>2</sup>Key Laboratory of Material Simulation Methods and Software of Ministry of Education, College of Physics, Jilin University, Changchun 130012, China

<sup>3</sup>Key Laboratory of Physics and Technology for Advanced Batteries (Ministry of Education), International Center of Future Science, Jilin University, Changchun 130012, China

 (Received 16 August 2023; revised 18 October 2023; accepted 20 November 2023; published 13 December 2023)

Since the discovery of superconductivity, the realization of room-temperature superconductivity has been the long dream of mankind. Recently, it has been reported that nitrogen-doped lutetium hydride has room-temperature superconductivity at near-ambient conditions. However, there is no solid evidence of such tantalizing superconductivity in nitrogen-doped lutetium hydride synthesized by follow-up experiments. The compositions and crystal structures of the nitrogen-doped lutetium hydride are still unclear. Therefore, we here systematically study the structural stability and electronic properties of  $Fm\bar{3}m$  LuH<sub>3</sub> and N-doped  $Fm\bar{3}m$  LuH<sub>3</sub>, such as 1, 2, 3, 4, and 8% N, by first-principles calculations. Our further electronic properties calculations show that all the simulated Lu-N-H ternary compounds are metallic, except for a semiconducting phase of Lu<sub>4</sub>H<sub>11</sub>N (LuH<sub>2.75</sub>N<sub>0.25</sub>). Remarkably, the contribution of the H atoms to the electronic density of states at the Fermi level could be tuned by the increasing N concentration. Electron-phonon coupling calculations also show that both  $Fm\bar{3}m$  LuH<sub>3</sub> and  $Pm\bar{3}m$  Lu<sub>4</sub>H<sub>11</sub>N are superconducting with critical temperature  $T_c$ 's of 23 and 32 K at 24 and 60 GPa, respectively. Our current results suggest that LuH<sub>3</sub> and N-doped LuH<sub>3</sub> could be potential superconductors only at high pressure, while the estimated  $T_c$  values are much lower than room temperature.

DOI: [10.1103/PhysRevResearch.5.043238](https://doi.org/10.1103/PhysRevResearch.5.043238)

### I. INTRODUCTION

Hunting room-temperature superconductivity has been the goal of scientists since the discovery of superconductivity at  $\sim 4$  K for Hg [1]. In the past decade, hydrogen-based compounds have emerged as promising candidates for high-temperature superconductors [2–26]. Among them, the predicted cubic H<sub>3</sub>S was synthesized and confirmed to have a very high  $T_c$  of 203 K at 155 GPa [13,14]. Later, many other binary hydrides such as CaH<sub>6</sub> (210–215 K at 160–172 GPa) [15,16] and LaH<sub>10</sub> (250 K at 170 GPa) [17] have been measured with  $T_c > 200$  K [18–21]. Very recently, a series of ternary alloy hydrides has also been synthesized, including La-Y-H [22,23], La-Ce-H [24,25], and La-Be-H [26] compounds, which possess comparable  $T_c$ 's and lower stable pressures compared with those of similar binary hydrides.

Experimenters claimed that the N-doped lutetium hydride has a  $T_c$  of  $\sim 294$  K at only 1 GPa [27]. The reported  $T_c$  is surprisingly high, close to room temperature, while the

required pressure is several orders of magnitude lower than previously demonstrated for hydrides [15–26], close to near-ambient pressure. Subsequently, numerous experimental and theoretical studies on Lu-H and Lu-N-H systems were continuously reported [28–49]. In experiment, binary LuH<sub>3</sub> and Lu<sub>4</sub>H<sub>23</sub> are reported to be superconducting with  $T_c$  of 12.4 and 71 K at very high pressures of 122 and 218 GPa, respectively [28,29]. Shan *et al.* [30] observed a color change in the LuH<sub>2</sub> sample, but no superconductivity was found  $> 1.5$  K. For the ternary Lu-N-H system, Cai *et al.* [31] prepared a sample from the lutetium foil and H<sub>2</sub>/N<sub>2</sub> gas mixture and performed high-pressure resistance and magnetic susceptibility measurements, but no superconductivity was found. Using different preparations from Ref. [31], two independent groups synthesized Lu-N-H samples and concluded that there is no superconductivity at pressures up to 50.5 GPa and temperatures down to 1.8 K [32–34].

In theory,  $Fm\bar{3}m$  LuH<sub>3</sub> is calculated to be dynamically unstable at ambient pressure within harmonic approximation, while it can be stabilized at 0 GPa ( $T > 200$  K) or 6 GPa ( $T > 80$  K) when temperature and quantum anharmonic lattice effects are included [36,37]. Within the Migdal-Eliashberg formalism, using temperature- and quantum-anharmonically corrected phonon dispersions, the calculated  $T_c$  for  $Fm\bar{3}m$  LuH<sub>3</sub> is  $\sim 50 - 60$  K (at 2.8 GPa and 300 K) and 19 K (at 6 GPa and 300 K) [36,37], respectively. Through structural searches, only Lu<sub>4</sub>N<sub>2</sub>H<sub>5</sub>

\*gaogyoying@ysu.edu.cn

Published by the American Physical Society under the terms of the Creative Commons Attribution 4.0 International license. Further distribution of this work must maintain attribution to the author(s) and the published article's title, journal citation, and DOI.

is predicted to be thermodynamically stable [38–43], but with an estimated  $T_c$  of  $\sim 0$  at 5 GPa [38]. Using the virtual crystal approximation method, several Lu-N-H unstoichiometries have been studied [43], with the highest  $T_c$  of 22 K obtained with 1% N-doping at 30 GPa. With the supercell method, some Lu-N-H stoichiometries,  $\text{Lu}_4\text{H}_m\text{N}_{12-m}$  and  $\text{Lu}_8\text{H}_{23-x}\text{N}$  have been built by doping nitrogen in  $Fm\bar{3}m$   $\text{LuH}_3$  [43–47]. However, the full Brillouin zone (BZ) electron-phonon coupling (EPC) calculations have been performed only for  $\text{Lu}_2\text{H}_2\text{N}$  ( $\text{LuHN}_{0.5}$ ) and  $\text{Lu}_4\text{H}_{10}\text{N}_2$  ( $\text{LuH}_{2.5}\text{N}_{0.5}$ ), which are estimated to possess  $T_c$ 's of 0.2 and 27 K at 0 and 50 GPa, respectively [43]. Until now, the crystal structures and electronic properties of different N concentrations doped in  $Fm\bar{3}m$   $\text{LuH}_3$  and their relationships with the parent  $Fm\bar{3}m$   $\text{LuH}_3$  have not been systematically investigated, especially over a wider range of N-doping concentrations rather than a narrower range, or a single concentration.

In this paper, we obtained hitherto unknown  $\text{Lu}_4\text{H}_{11}\text{N}$ ,  $\text{Lu}_8\text{H}_{23}\text{N}$ ,  $\text{Lu}_{12}\text{H}_{35}\text{N}$ ,  $\text{Lu}_{16}\text{H}_{47}\text{N}$ , and  $\text{Lu}_{32}\text{H}_{95}\text{N}$  stoichiometries using supercell method by doping N in cubic  $Fm\bar{3}m$   $\text{LuH}_3$  as well as the further in-depth investigation of the influence for different doping concentrations on their structural stability and electronic properties based on first-principles calculations. We found that the calculated x-ray diffraction (XRD) patterns of  $Pm\bar{3}m$   $\text{Lu}_4\text{H}_{11}\text{N}$ ,  $P4/mmm-1$   $\text{Lu}_{16}\text{H}_{47}\text{N}$ ,  $P\bar{4}3m$   $\text{Lu}_{32}\text{H}_{95}\text{N}$ , and  $Pm\bar{3}m$   $\text{Lu}_{32}\text{H}_{95}\text{N}$  show good agreement with experimental results [27] for the principal diffraction peaks. Furthermore,  $Fm\bar{3}m$   $\text{LuH}_3$  and  $Pm\bar{3}m$   $\text{Lu}_4\text{H}_{11}\text{N}$  are dynamically stable at pressures  $>24$  and 60 GPa, with predicted  $T_c$ 's of 23 and 32 K, respectively, which is far lower than that reported in experiment with implication of the observed room-temperature superconductivity unlikely.

## II. COMPUTATIONAL DETAILS

The structural relaxations and electronic properties were performed using the Vienna *ab initio* simulation package based on density functional theory (DFT) with the Perdew-Burke-Ernzerhof generalized gradient approximation [48,49]. The ion-electron interaction was described by projector augmented-wave (PAW) potentials, where  $1s^1$ ,  $4f^{14}5s^25p^65d^16s^2$ , and  $2s^22p^3$  configurations were treated as valence electrons for H, Lu, and N atoms, respectively [50]. The plane-wave kinetic energy cutoff was set to 800 eV, and corresponding Monkhorst-Pack (MP)  $k$ -point meshes for different structures were adopted to ensure that the enthalpy converges to several mellelectronvolts per atom. Furthermore, the Heyd-Scuseria-Ernzerhof (HSE) [51] functional was employed for  $Fm\bar{3}m$   $\text{LuH}_3$ . We used DFT and DFT+ $U$  [52,53] (with  $U=5.5$  eV) to calculate the lattice parameters of  $Fm\bar{3}m$   $\text{LuH}_3$  at low pressures, and the results are shown in Fig. S1 in the Supplemental Material (SM) [54]. The DFT results without the Hubbard  $U$  effect are close to the experimental data [55]. Therefore, the DFT-level calculations of  $\text{LuH}_3$  and Lu-N-H compounds were used. In addition, we calculated the lattice parameters of  $Fm\bar{3}m$   $\text{LuH}_3$  and  $Pm\bar{3}m$   $\text{Lu}_4\text{NH}_{11}$  with and without spin-orbit coupling (SOC) at 60 GPa, respectively. As shown in Table S1 in the SM [54], the lattice structures were not altered by considering SOC effects. SPAP [56] was employed to analyze symmetries, compare similar-

ties of large numbers of crystal structures, and automatically classify the structures into groups. The reference phases to compute the enthalpy difference diagram are consistent with The Material Project, which uses the  $P\bar{3}c1$  phase for  $\text{LuH}_3$ , the  $Fm\bar{3}m$  phase for  $\text{LuH}_2$ , the  $Fm\bar{3}m$  phase for LuN, and the  $P2_13$  and  $P2_12_12_1$  phases for  $\text{NH}_3$ . Phonon calculations were performed by using PHONOPY [57] or QUANTUM ESPRESSO code [58]. EPC calculations were carried out through QUANTUM ESPRESSO, using PAW pseudopotentials for all atoms. The kinetic energy cutoff adopted 75 Ry, and  $6\times 6\times 6$  and  $9\times 9\times 9$   $q$ -point meshes in the first BZ were used for  $Pm\bar{3}m$   $\text{Lu}_4\text{NH}_{11}$  and  $Fm\bar{3}m$   $\text{LuH}_3$ , respectively. Correspondingly, we chose MP grids of  $24\times 24\times 24$  and  $36\times 36\times 36$  to ensure  $k$ -point sampling convergence.

## III. RESULTS AND DISCUSSION

As the low nitrogen-doped Lu-H system is reported in the room-temperature superconductivity experiment, here, we set up different Lu-N-H stoichiometries to mimic the experimental sample using the supercell method. Based on a conventional cell of  $Fm\bar{3}m$   $\text{LuH}_3$ , including 4 f.u., we first built different sizes of supercells, and then a nitrogen atom replaced a hydrogen atom at any site in each supercell. Five different Lu-N-H stoichiometries  $\text{Lu}_4\text{H}_{11}\text{N}$  ( $\text{LuH}_{2.75}\text{N}_{0.25}$ ),  $\text{Lu}_8\text{H}_{23}\text{N}$  ( $\text{LuH}_{2.875}\text{N}_{0.125}$ ),  $\text{Lu}_{12}\text{H}_{35}\text{N}$  ( $\text{LuH}_{2.917}\text{N}_{0.083}$ ),  $\text{Lu}_{16}\text{H}_{47}\text{N}$  ( $\text{LuH}_{2.9375}\text{N}_{0.0625}$ ), and  $\text{Lu}_{32}\text{H}_{95}\text{N}$  ( $\text{LuH}_{2.96875}\text{N}_{0.03125}$ ) were obtained corresponding to N concentrations of 8, 4, 3, 2, and 1%, respectively. Two different structures are obtained for each stoichiometry by the SPAP procedure or by exhaustive enumeration (Table S2 in the SM [54]). The  $P4/mmm$  or  $Pm\bar{3}m$  structure and  $P\bar{4}2m$  or  $P\bar{4}3m$  structure are obtained by replacing one hydrogen atom located in the octahedral or tetrahedral site of  $Fm\bar{3}m$   $\text{LuH}_3$  supercells with one nitrogen atom, respectively. As a result, the  $P\bar{4}3m$  and  $Pm\bar{3}m$ ,  $P4/mmm$  and  $P\bar{4}2m$ ,  $P4/mmm$  and  $P\bar{4}2m$ ,  $P4/mmm$  and  $P\bar{4}2m$ , and  $P\bar{4}3m$  and  $Pm\bar{3}m$  structures are obtained for  $\text{Lu}_4\text{H}_{11}\text{N}$ ,  $\text{Lu}_8\text{H}_{23}\text{N}$ ,  $\text{Lu}_{12}\text{H}_{35}\text{N}$ ,  $\text{Lu}_{16}\text{H}_{47}\text{N}$ , and  $\text{Lu}_{32}\text{H}_{95}\text{N}$ , respectively. The crystal structures for different stoichiometries are shown in Figs. 1 and S2 in the SM [54]. Detailed information on the structural parameters is listed in Table S3 in the SM [54]. In addition, the ambient-pressure  $P\bar{3}c1$  and high-pressure  $Fm\bar{3}m$  structures for  $\text{LuH}_3$  are listed in Fig. 1.

As for the thermodynamic stability of our simulated structures, the relative enthalpies with respect to the known binary compounds and the corresponding elemental solid are presented in Figs. 2 and S3 in the SM [54]. As a result, these structures are thermodynamically metastable at the considered pressure range. For  $\text{Lu}_4\text{H}_{11}\text{N}$ ,  $P\bar{4}3m$  is enthalpically stable  $<75$  GPa, above which  $Pm\bar{3}m$  becomes stable [Fig. 2(a)]. For  $\text{Lu}_8\text{H}_{23}\text{N}$ , the  $P\bar{4}2m$  structure is more enthalpically advantageous than the  $Cmmm$  structure proposed by Denchfield *et al.* [45] at pressures  $<12$  GPa [Fig. 2(b)]. As the pressure increases, the  $Cmmm$  structure becomes stable. For  $\text{Lu}_{12}\text{H}_{35}\text{N}$  and  $\text{Lu}_{16}\text{H}_{47}\text{N}$ , the  $P\bar{4}2m$  structure is lower in enthalpy once the pressure is  $<31$  and 20 GPa, respectively, and then the  $P4/mmm$  phase becomes lower. For  $\text{Lu}_{32}\text{H}_{95}\text{N}$ , the intersections of the enthalpy-pressure curves of different structures in Fig. 2(d) show that the phase transition pressure from the

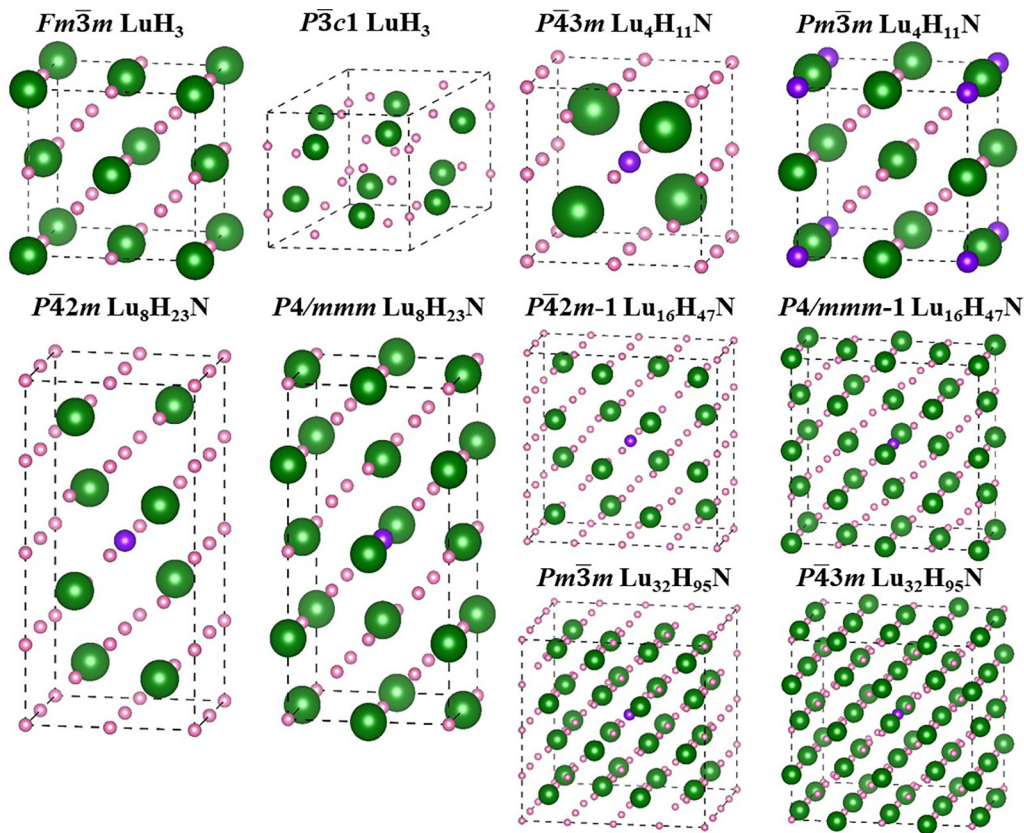


FIG. 1. The crystal structures of binary  $\text{LuH}_3$  and ternary Lu-N-H hydrides. Green, pink, and purple balls represent Lu, H, and N atoms, respectively.

$Pm\bar{3}m$  to the  $P\bar{4}3m$  structure is 11 GPa. For  $\text{LuH}_3$ , the phase transition from the  $P\bar{3}c1$  to the  $Fm\bar{3}m$  structure is calculated to occur at 26 GPa (Fig. S3(a) in the SM [54]), which is in good agreement with the previously theoretical result of 25 GPa [36] and the experimental result of 26.2 GPa [47].

We also investigated the dynamical stability of  $\text{LuH}_3$  and the ternary Lu-N-H hydrides by calculating their phonon spectra at the level of harmonic theory. As shown in Figs. 3 and S4 in the SM [54], the lack of imaginary frequencies in the calculated phonon dispersion curves indicates that all structures are dynamically stable at the corresponding pressures. Moreover, these Lu-N-H hydrides can be dynamically stable to 100 GPa, as shown in Fig. S5 in the SM [54]. We give the minimum dynamically stable pressures of Lu-N-H hydrides as a function of N-doping concentration, as shown in Fig. S6 in the SM [54]. We find that the minimum dynamically stable pressures are much lower for N concentrations between 2 and 4%, and N concentration of 3% has the lowest dynamically stable pressure of 10 GPa. Comparing with the results of Huo *et al.* [43] by the virtual crystal approximation method, our calculated minimum dynamically stable pressure for Lu-N-H compounds by the supercell method does not increase monotonically with the increasing N concentration in the pressure range we studied. Notably, as demonstrated for some hydrogen-rich compounds, anharmonicity and the quantum motion of ions, which are also neglected in the harmonic phonon calculations of the Born-Oppenheimer approximation, could have significant effects [60–63]. Some studies have demonstrated that  $Fm\bar{3}m$   $\text{LuH}_3$

can be dynamically stable at 0 GPa ( $T > 200$  K) or 6 GPa ( $T > 80$  K) when temperature and quantum anharmonic lattice effects are included [36,37]. Thus, anharmonic and temperature effects may reduce the dynamically stable pressure of N-doped  $\text{LuH}_3$ , but it is unlikely to alter the conclusion of this paper.

We further calculated the XRD patterns for these Lu-N-H compounds. Figures 4 and S7 in the SM [54] show a comparison of the experimental and calculated XRD patterns. The simulated principal diffraction peaks of  $Pm\bar{3}m$   $\text{Lu}_4\text{H}_{11}\text{N}$ ,  $P4/mmm-1$   $\text{Lu}_{16}\text{H}_{47}\text{N}$ ,  $P\bar{4}3m$   $\text{Lu}_{32}\text{H}_{95}\text{N}$ , and  $Pm\bar{3}m$   $\text{Lu}_{32}\text{H}_{95}\text{N}$  are in good agreement with those observed in experiment [27]. In addition, the intensity ratio between the first and second principle peaks of  $P4/mmm-1$   $\text{Lu}_{16}\text{H}_{47}\text{N}$  is much closer to the experimental results. These results indicate that our simulated structures could be the microstructure of the sample observed in experiment.

To investigate the metallic properties as observed in experiment, the electronic band structures and density of states (DOS) for  $Fm\bar{3}m$   $\text{LuH}_3$  and  $Pm\bar{3}m$   $\text{Lu}_4\text{H}_{11}\text{N}$  as well as for other Lu-N-H compounds are calculated, as shown in Figs. 5, 6, and Fig. S10 in the SM [54]. In the electronic band structures, both  $Fm\bar{3}m$   $\text{LuH}_3$  and  $Pm\bar{3}m$   $\text{Lu}_4\text{H}_{11}\text{N}$  have energy bands that cross the Fermi level, revealing the metallic feature of these simulated structures. The contributions from H to the energy bands, especially at the Fermi level, are more obvious when N is introduced into the  $\text{LuH}_3$  lattice. Considering the different functionals and SOC might play a role in electronic

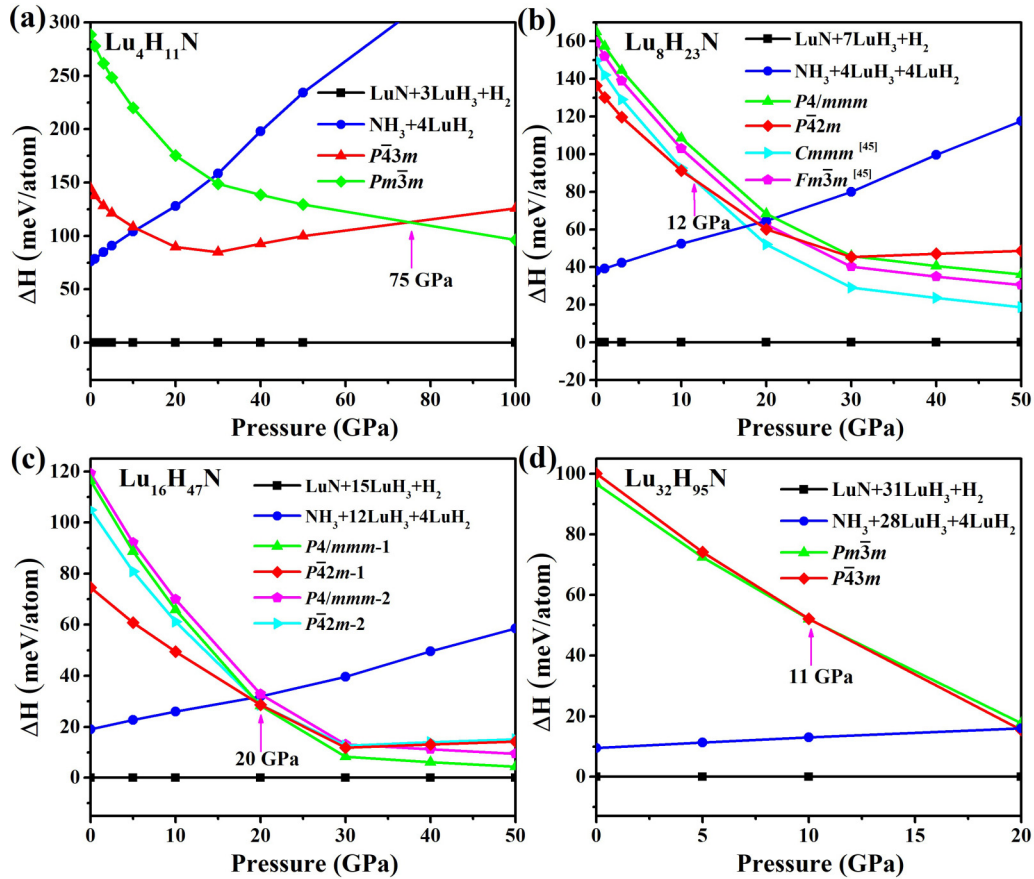


FIG. 2. Enthalpy curves per atom as a function of pressure for (a)  $\text{Lu}_4\text{H}_{11}\text{N}$ , (b)  $\text{Lu}_8\text{H}_{23}\text{N}$ , (c)  $\text{Lu}_{16}\text{H}_{47}\text{N}$ , and (d)  $\text{Lu}_{32}\text{H}_{95}\text{N}$ , respectively. The following structures were considered for the known binary compounds and the corresponding elemental solid:  $P\bar{3}c1$  and  $Fm\bar{3}m$  for  $\text{LuH}_3$  [28],  $Fm\bar{3}m$  for  $\text{LuH}_2$ ,  $Fm\bar{3}m$  for  $\text{LuN}$ ,  $P2_13$  and  $P2_12_12_1$  for  $\text{NH}_3$ , and  $P6_3/m$  for  $\text{H}_2$  [59].

properties of  $Fm\bar{3}m$   $\text{LuH}_3$  and  $Pm\bar{3}m$   $\text{Lu}_4\text{H}_{11}\text{N}$ , we studied the effects of the HSE functional and SOC on their electronic

band structures at 60 GPa. The calculated band structures for  $Fm\bar{3}m$   $\text{LuH}_3$  with HSE suggest the metallic feature as well, as shown in Fig. S8 in the SM [54]. In addition, the shapes of the electronic band structures for  $Fm\bar{3}m$   $\text{LuH}_3$  and  $Pm\bar{3}m$   $\text{Lu}_4\text{H}_{11}\text{N}$  with and without SOC are similar, except for the energy bands split by SOC, as expected (Fig. S9 in the SM [54]). Therefore, both  $\text{LuH}_3$  and  $\text{Lu}_4\text{H}_{11}\text{N}$  are metal with or without SOC. In Figs. 6 and S10 in the SM [54], the calculated projected DOS shows the presence of electronic states at the Fermi level except  $P\bar{4}3m$   $\text{Lu}_4\text{H}_{11}\text{N}$ , indicating that these hydrides are all metallic in the range of pressures studied. For  $Fm\bar{3}m$   $\text{LuH}_3$ , the Lu atoms contribute mainly to the total DOS at the Fermi level and a very small contribution from the H atoms, indicating unfavorable to high-temperature superconductivity, as shown for many binary hydrides such as  $\text{NbH}_2$ ,  $\text{ScH}_3$  [64,65]. With the incorporation of an N atom, the contribution of H atoms to the DOS at the Fermi level increases significantly for  $Pm\bar{3}m$   $\text{Lu}_4\text{H}_{11}\text{N}$ , by comparing with  $Fm\bar{3}m$   $\text{LuH}_3$ . As the N concentration increases from 1 to 8%, the contribution of the H atoms to the electronic DOS at the Fermi level tends to increase nearly fourfold, suggesting that the superconducting transition temperature might also increase at the studied 60 GPa.

Due to the metallic feature of pure and N-doped  $\text{LuH}_3$ , we then explore their superconducting properties within the cor-

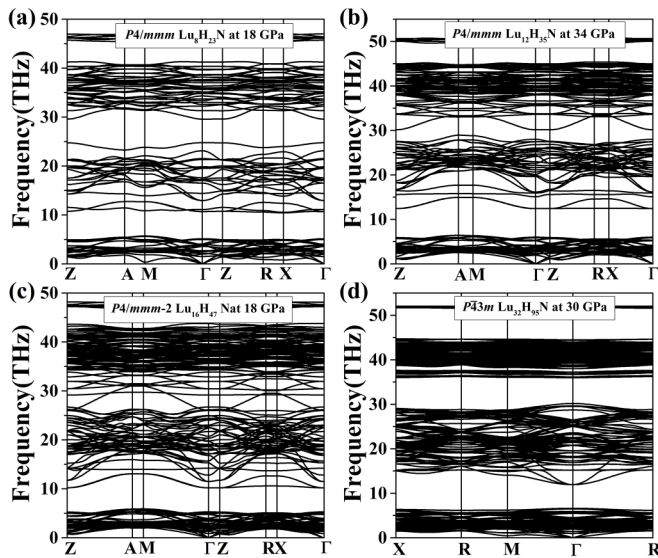


FIG. 3. Phonon dispersion relations for (a)  $P4/mmm$   $\text{Lu}_8\text{H}_{23}\text{N}$ , (b)  $P4/mmm$   $\text{Lu}_{12}\text{H}_{35}\text{N}$ , (c)  $P4/mmm-2$   $\text{Lu}_{16}\text{H}_{47}\text{N}$ , and (d)  $P\bar{4}3m$   $\text{Lu}_{32}\text{H}_{95}\text{N}$ .

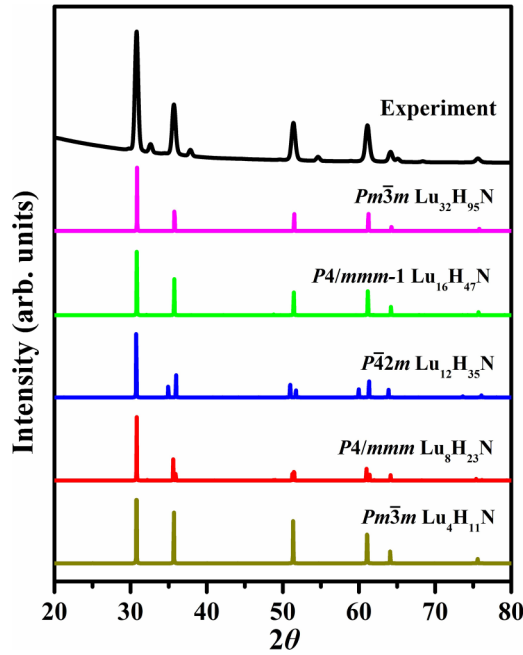


FIG. 4. Simulated XRD patterns compared with the experimental results reported by Dasenbrock-Gammon *et al.* [27] for  $Pm\bar{3}m$   $\text{Lu}_{32}\text{H}_{95}\text{N}$ ,  $P4/mmm-1$   $\text{Lu}_{16}\text{H}_{47}\text{N}$ ,  $P\bar{4}2m$   $\text{Lu}_{12}\text{H}_{35}\text{N}$ ,  $P4/mmm$   $\text{Lu}_8\text{H}_{23}\text{N}$ , and  $Pm\bar{3}m$   $\text{Lu}_4\text{H}_{11}\text{N}$ . The small peaks of experimentally measured XRD might be from other possible compounds of  $\text{LuN} + \text{Lu}_2\text{O}_3$ .

responding dynamically stable pressure range. For the ternary Lu-N-H stoichiometries, we take  $Pm\bar{3}m$   $\text{Lu}_4\text{H}_{11}\text{N}$  as a representative example since its hydrogen atoms contribute most to the electronic DOS at the Fermi level. We then calculated the EPC parameter  $\lambda$ , phonon frequency logarithmic average  $\omega_{\log}$ , and the superconducting critical temperature  $T_c$  for  $Fm\bar{3}m$   $\text{LuH}_3$  and  $Pm\bar{3}m$   $\text{Lu}_4\text{H}_{11}\text{N}$  at 60 GPa, respectively (Table I). The  $T_c$  values were calculated by the Allen-Dynes modified McMillan equation [66] with  $\mu^*$  of 0.1–0.13. According to our calculations, the calculated EPC parameter  $\lambda$  and phonon frequency logarithmic average  $\omega_{\log}$  of  $Fm\bar{3}m$   $\text{LuH}_3$  is 0.96 and 340 K at 24 GPa, resulting in a  $T_c$  of 23 K with  $\mu^* = 0.1$ , which agrees with the other theoretical results of 16 K [43]. When the pressure increases from 24 to 60 GPa, the calculated

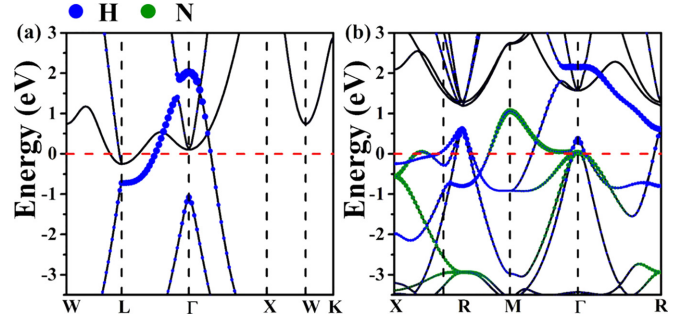


FIG. 5. Calculated electronic band structures of  $Fm\bar{3}m$   $\text{LuH}_3$  and  $Pm\bar{3}m$   $\text{Lu}_4\text{H}_{11}\text{N}$  at 24 and 60 GPa, respectively. The atomic contributions of H and N to bands are also displayed in the band structures.

$\lambda$  for  $Fm\bar{3}m$   $\text{LuH}_3$  decreases from 0.96 to 0.41, whereas  $\omega_{\log}$  increases from 340 to 645 K. As a result of these two effects, the calculated  $T_c$  decreases from 23 to 3.2 K, assuming  $\mu^* = 0.1$ . For  $Pm\bar{3}m$   $\text{Lu}_4\text{H}_{11}\text{N}$ , it has EPC interactions with  $\lambda$  of 3.16 and  $\omega_{\log}$  of 176 K at 60 GPa. The  $T_c$  value was estimated to be 32 K with  $\mu^* = 0.1$ . The  $T_c$  value of  $Pm\bar{3}m$   $\text{Lu}_4\text{H}_{11}\text{N}$  is 10 times larger than that of  $Fm\bar{3}m$   $\text{LuH}_3$  at 60 GPa, which is also consistent with the electronic DOS contribution from the H atoms. We also calculated the superconducting properties of  $Fm\bar{3}m$   $\text{LuH}_3$  under higher pressure and estimated its  $T_c$  to be 0.2 K at 120 GPa, which is much lower than the experimentally measured 12.4 K under the conditions of 122 GPa and 300 K [28]. This discrepancy between theory and experiment might be partly attributed to quantum anharmonic and temperature effects. Two other theoretical results also show that  $T_c$  will increase to 19 and 50–60 K when the pressure decreases to 6 and 2.8 GPa at 300 K, respectively.

To understand the origin of the EPC, we calculated their phonon spectra, projected phonon DOS, Eliashberg phonon spectral function  $\alpha^2F(\omega)/\omega$ , and integral  $\lambda(\omega)$ . As shown in Fig. 7, for  $Fm\bar{3}m$   $\text{LuH}_3$ , the contribution to  $\lambda$  of the vibrations related to Lu atoms is lower than that of vibrations related to H atoms at 60 GPa. When the N atom is introduced, in  $Pm\bar{3}m$   $\text{Lu}_4\text{H}_{11}\text{N}$ , the vibrations related to Lu atoms in the range of 1–6 THz contribute the most to  $\lambda$ , accounting for 67% of the total value, while the contribution related to vibrations of N atoms in the range of 14–17 THz accounts for 17% of the

TABLE I. The calculated EPC parameter  $\lambda$ , phonon frequency logarithmic average  $\omega_{\log}$ , and critical temperature  $T_c$  ( $\mu^* = 0.1 - 0.13$ ) from the Allen-Dynes modified McMillan equation for  $Fm\bar{3}m$   $\text{LuH}_3$  and  $Pm\bar{3}m$   $\text{Lu}_4\text{H}_{11}\text{N}$ .

Phase	$P$ (GPa)	$\lambda$	$\omega_{\log}$ (K)	$T_c$ (K) $\mu^* = 0.1 - 0.13$ , McMillan
$\text{LuH}_3$ ( $Fm\bar{3}m$ )	24	0.96	340	23–20
$\text{LuH}_3$ ( $Fm\bar{3}m$ )	60	0.41	645	3.2–1.5
$\text{LuH}_3$ ( $Fm\bar{3}m$ )	120	0.29	682	0.20–0.03
$\text{Lu}_4\text{H}_{11}\text{N}$ ( $Pm\bar{3}m$ )	60	3.16	176	32–31
$\text{LuH}_3$ ( $Fm\bar{3}m$ ) [38]	0	1.70	17.6 (meV)	25.4 ( $\mu^* = 0.1$ )
$\text{LuH}_3$ ( $Fm\bar{3}m$ ) [43]	25	0.82	328	16–13
$\text{LuH}_3$ ( $Fm\bar{3}m$ ) [43]	50	0.44	667	4–2
$\text{LuH}_3$ ( $Fm\bar{3}m$ ) [37]	6 (300 K)	—	—	19 (Eliashberg)
$\text{LuH}_3$ ( $Fm\bar{3}m$ ) [36]	2.8 (300 K)	1.7	—	50–60 (Eliashberg)
$\text{LuH}_3$ ( $Fm\bar{3}m$ ) [28]	122	—	—	12.4 (Exp.)

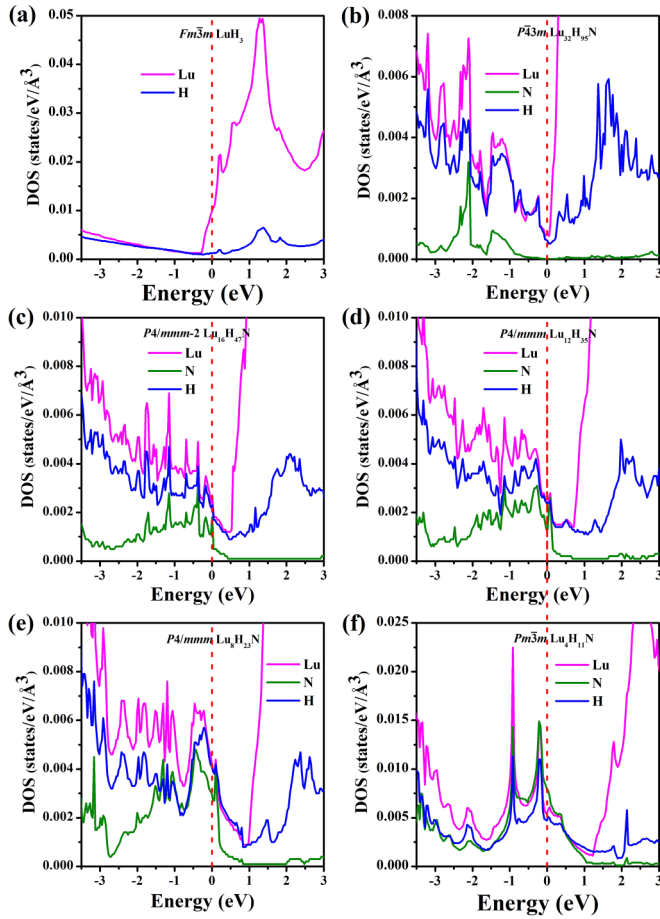


FIG. 6. Calculated electronic density of states for Lu-N-H compounds at 60 GPa.

total value. Interestingly, doping by nitrogen atoms at 8% concentration increases  $\lambda$  from 0.41 to a remarkable value of 3.16. Thus, the increase in  $T_c$  of N-doped  $\text{LuH}_3$  is mainly caused by an increase in the  $\lambda$  value. These results indicate that the N doping could significantly alter the electrical behavior of the Lu-H system, which might explain the electrical drop behavior of the sample in experiment owing to the change of N-doped concentration.

#### IV. CONCLUSIONS

We systematically explored the structural stability and electronic properties of pure and N-doped  $\text{LuH}_3$  under pressure based on first-principles calculations. The results show that all the Lu-N-H compounds can be dynamically stable at certain pressures. Among them,  $P4_2m \text{Lu}_{12}\text{H}_{35}\text{N}$  ( $\text{LuH}_{2.917}\text{N}_{0.083}$ ) can be dynamically stable at a pressure as low as 10 GPa. The calculated XRD patterns of  $Pm\bar{3}m \text{Lu}_4\text{H}_{11}\text{N}$ ,  $P4/mmm-1 \text{Lu}_{16}\text{H}_{47}\text{N}$ ,  $P\bar{4}3m \text{Lu}_{32}\text{H}_{95}\text{N}$ , and

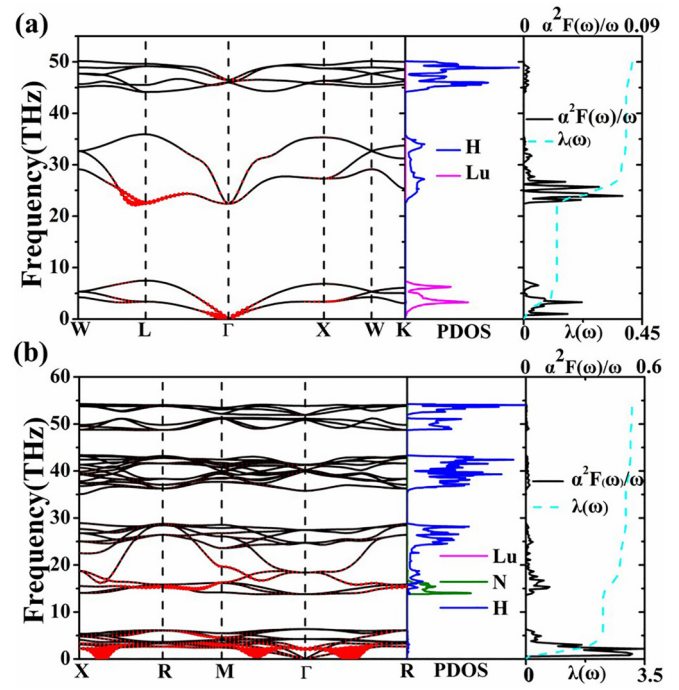


FIG. 7. Calculated phonon dispersion curves [red circle area proportional to associated EPC], PDOS, the Eliashberg phonon spectral function  $\alpha^2 F(\omega)/\omega$ , and its integral  $\lambda(\omega)$  of (a)  $Fm\bar{3}m \text{LuH}_3$  and (b)  $Pm\bar{3}m \text{Lu}_4\text{H}_{11}\text{N}$  at 60 GPa, respectively.

$Pm\bar{3}m \text{Lu}_{32}\text{H}_{95}\text{N}$  are in good agreement with experimental results for the principal diffraction peaks. Electronic properties calculations reveal that all the Lu-N-H compounds are metallic, except that  $P\bar{4}3m \text{Lu}_4\text{H}_{11}\text{N}$  ( $\text{LuH}_{2.75}\text{N}_{0.25}$ ) is a semi-conducting phase. As the N concentration increases from 1 to 8%, the contribution of the H atoms to the electronic DOS at the Fermi level tends to increase. Here,  $Fm\bar{3}m \text{LuH}_3$  and  $Pm\bar{3}m \text{Lu}_4\text{H}_{11}\text{N}$  are dynamically stable at pressures as low as 24 and 60 GPa, with the estimated  $T_c$ 's of 23 and 32 K, respectively. Also,  $Fm\bar{3}m \text{LuH}_3$  and N-doped  $Fm\bar{3}m \text{LuH}_3$  can both be superconducting phases only at high pressure, but the estimated  $T_c$  values are still far lower than reported room temperature, indicating the unreliability of the experimental results.

#### ACKNOWLEDGMENTS

We thank Professor Lin Wang and Dr. Yuefeng Wang from Center for High Pressure Science and State Key Laboratory of Metastable Materials Science and Technology (Yanshan University) for their helpful suggestions and discussions. This paper was supported by Natural Science Foundation of China (Grants No. 52022089, No. 52372261, No. 52288102, and No. 12074138).

[1] H. K. Onnes, Further experiments with liquid helium. C. On the change of electric resistance of pure metals at very low

temperatures etc. IV. The resistance of pure mercury at helium temperatures, in *Through Measurement to Knowledge*.

- Boston Studies in the Philosophy of Science, Vol 124, edited by K. Gavroglu and Y. Goudaroulis (Springer, Dordrecht, 1991), pp. 261.
- [2] G. Gao, A. R. Oganov, A. Bergara, M. Martinez-Canales, T. Cui, T. Iitaka, Y. Ma, and G. Zou, Superconducting high pressure phase of germane, *Phys. Rev. Lett.* **101**, 107002 (2008).
- [3] G. Gao, H. Wang, A. Bergara, Y. Li, G. Liu, and Y. Ma, Metallic and superconducting gallane under high pressure, *Phys. Rev. B* **84**, 064118 (2011).
- [4] H. Wang, J. S. Tse, K. Tanaka, T. Iitaka, and Y. Ma, Superconductive sodalite-like clathrate calcium hydride at high pressures, *Proc. Natl. Acad. Sci. USA* **109**, 6463 (2012).
- [5] D. Duan, Y. Liu, F. Tian, D. Li, X. Huang, Z. Zhao, H. Yu, B. Liu, W. Tian, and T. Cui, Pressure-induced metallization of dense  $(\text{H}_2\text{S})_2\text{H}_2$  with high- $T_c$  superconductivity, *Sci. Rep.* **4**, 6968 (2014).
- [6] H. Liu, I. I. Naumov, R. Hoffmann, N. W. Ashcroft, and R. J. Hemley, Potential high- $T_c$  superconducting lanthanum and yttrium hydrides at high pressure, *Proc. Natl. Acad. Sci. USA* **114**, 6990 (2017).
- [7] F. Peng, Y. Sun, C. J. Pickard, R. J. Needs, Q. Wu, and Y. Ma, Hydrogen clathrate structures in rare earth hydrides at high pressures: Possible route to room-temperature superconductivity, *Phys. Rev. Lett.* **119**, 107001 (2017).
- [8] G. Gao, L. Wang, M. Li, J. Zhang, R. T. Howie, E. Gregoryanz, V. V. Struzhkin, L. Wang, and J. S. Tse, Superconducting binary hydrides: Theoretical predictions and experimental progresses, *Mater. Today Phys.* **21**, 100546 (2021).
- [9] X. Liang, A. Bergara, L. Wang, B. Wen, Z. Zhao, X. Zhou, J. He, G. Gao, and Y. Tian, Potential high- $T_c$  superconductivity in  $\text{CaYH}_{12}$  under pressure, *Phys. Rev. B* **99**, 100505(R) (2019).
- [10] X. Liang, A. Bergara, X. Wei, X. Song, L. Wang, R. Sun, H. Liu, R. J. Hemley, L. Wang, G. Gao *et al.*, Prediction of high- $T_c$  superconductivity in ternary lanthanum borohydrides, *Phys. Rev. B* **104**, 134501 (2021).
- [11] X. Wei, X. Hao, A. Bergara, E. Zurek, X. Liang, L. Wang, X. Song, P. Li, L. Wang, G. Gao *et al.*, Designing ternary superconducting hydrides with A15-type structure at moderate pressures, *Mater. Today Phys.* **34**, 101086 (2023).
- [12] X. Liang, X. Wei, E. Zurek, A. Bergara, P. Li, G. Gao, and Y. Tian, Design of high-temperature at moderate pressures by alloying  $\text{AlH}_3$  or  $\text{GaH}_3$ , *Matter Radiat. Extremes* **9**, 018401 (2024).
- [13] A. P. Drozdov, M. I. Eremets, I. A. Troyan, V. Ksenofontov, and S. I. Shylin, Conventional superconductivity at 203 kelvin at high pressures in the sulfur hydride system, *Nature (London)* **525**, 73 (2015).
- [14] M. Einaga, M. Sakata, T. Ishikawa, K. Shimizu, M. I. Eremets, A. P. Drozdov, I. A. Troyan, N. Hirao, and Y. Ohishi, Crystal structure of the superconducting phase of sulfur hydride, *Nat. Phys.* **12**, 835 (2016).
- [15] L. Ma, K. Wang, Y. Xie, X. Yang, Y. Wang, M. Zhou, H. Liu, X. Yu, Y. Zhao, H. Wang *et al.*, High-temperature superconducting phase in clathrate calcium hydride  $\text{CaH}_6$  up to 215 K at a pressure of 172 GPa, *Phys. Rev. Lett.* **128**, 167001 (2022).
- [16] Z. Li, X. He, C. Zhang, X. Wang, S. Zhang, Y. Jia, S. Feng, K. Lu, J. Zhao, J. Zhang *et al.*, Superconductivity above 200 K discovered in superhydrides of calcium, *Nat. Commun.* **13**, 2863 (2022).
- [17] A. P. Drozdov, P. P. Kong, V. S. Minkov, S. P. Besedin, M. A. Kuzovnikov, S. Mozaffari, L. Balicas, F. F. Balakirev, D. E. Graf, V. B. Prakapenka *et al.*, Superconductivity at 250 K in lanthanum hydride under high pressures, *Nature (London)* **569**, 528 (2019).
- [18] I. A. Troyan, D. V. Semenov, A. G. Kvashnin, A. V. Sadakov, O. A. Sobolevskiy, V. M. Pudalov, A. G. Ivanova, V. B. Prakapenka, E. Greenberg, A. G. Gavriliuk *et al.*, Anomalous high-temperature superconductivity in  $\text{YH}_6$ , *Adv. Mater.* **33**, 2006832 (2021).
- [19] E. Snider, N. Dasenbrock-Gammon, R. McBride, X. Wang, N. Meyers, K. V. Lawler, E. Zurek, A. Salamat, and R. P. Dias, Synthesis of yttrium superhydride superconductor with a transition temperature up to 262 K by catalytic hydrogenation at high pressures, *Phys. Rev. Lett.* **126**, 117003 (2021).
- [20] P. Kong, V. S. Minkov, M. A. Kuzovnikov, A. P. Drozdov, S. P. Besedin, S. Mozaffari, L. Balicas, F. F. Balakirev, V. B. Prakapenka, S. Chariton *et al.*, Superconductivity up to 243 K in the yttrium-hydrogen system under high pressure, *Nat. Commun.* **12**, 5075 (2021).
- [21] D. V. Semenov, A. G. Kvashnin, A. G. Ivanova, V. Svitlyk, V. Yu. Fominski, A. V. Sadakov, O. A. Sobolevskiy, V. M. Pudalov, I. A. Troyan, and A. R. Oganov, Superconductivity at 161 K in thorium hydride  $\text{ThH}_{10}$ : Synthesis and properties, *Mater. Today* **33**, 36 (2020).
- [22] D. V. Semenov, I. A. Troyan, A. G. Ivanova, A. G. Kvashnin, I. A. Kruglov, M. Hanfland, A. V. Sadakov, O. A. Sobolevskiy, K. S. Pervakov, I. S. Lyubutin *et al.*, Superconductivity at 253 K in lanthanum-yttrium ternary hydrides, *Mater. Today* **48**, 18 (2021).
- [23] J. Bi, Y. Nakamoto, P. Zhang, Y. Wang, L. Ma, Y. Wang, B. Zou, K. Shimizu, H. Liu, M. Zhou *et al.*, Stabilization of superconductive La-Y alloy superhydride with  $T_c$  above 90 K at megabar pressure, *Mater. Today Phys.* **28**, 100840 (2022).
- [24] J. Bi, Y. Nakamoto, P. Zhang, K. Shimizu, B. Zou, H. Liu, M. Zhou, G. Liu, H. Wang, and Y. Ma, Giant enhancement of superconducting critical temperature in substitutional alloy  $(\text{La}, \text{Ce})\text{H}_9$ , *Nat. Commun.* **13**, 5952 (2022).
- [25] W. Chen, X. Huang, D. V. Semenov, S. Chen, D. Zhou, K. Zhang, A. R. Oganov, and T. Cui, Enhancement of superconducting properties in the La-Ce-H system at moderate pressures, *Nat. Commun.* **14**, 2660 (2023).
- [26] Y. Song, J. Bi, Y. Nakamoto, K. Shimizu, H. Liu, B. Zou, G. Liu, H. Wang, and Y. Ma, Stoichiometric ternary superhydride  $\text{LaBeH}_8$  as a new template for high-temperature superconductivity at 110 K under 80 GPa, *Phys. Rev. Lett.* **130**, 266001 (2023).
- [27] N. Dasenbrock-Gammon, E. Snider, R. McBride, H. Pasan, D. Durkee, N. Khalvashi-Sutter, S. Munasinghe, S. E. Dissanayake, K. V. Lawler, A. Salamat *et al.*, RETRACTED ARTICLE: Evidence of near-ambient superconductivity in a N-doped lutetium hydride, *Nature (London)* **615**, 244 (2023).
- [28] M. Shao, S. Chen, W. Chen, K. Zhang, X. Huang, and T. Cui, Superconducting  $\text{ScH}_3$  and  $\text{LuH}_3$  at megabar pressures, *Inorg. Chem.* **60**, 15330 (2021).
- [29] Z. Li, X. He, C. Zhang, K. Lu, B. Bin, J. Zhang, S. Zhang, J. Zhao, L. Shi, Y. Peng *et al.*, Superconductivity above 70 K experimentally discovered in lutetium polyhydride, *Sci. China Phys. Mech* **66**, 267411 (2023).

- [30] P. Shan, N. Wang, X. Zheng, Q. Qiu, Y. Peng, and J. Cheng, Pressure-induced color change in the lutetium dihydride LuH<sub>2</sub>, *Chin. Phys. Lett.* **40**, 046101 (2023).
- [31] S. Cai, J. Guo, H. Shu, L. Yang, P. Wang, Y. Zhou, J. Zhao, J. Han, Q. Wu, W. Yang *et al.*, No evidence of superconductivity in a compressed sample prepared from lutetium foil and H<sub>2</sub>/N<sub>2</sub> gas mixture, *Matter Radiat. Extremes* **8**, 048001 (2023).
- [32] X. Ming, Y. Zhang, X. Zhu, Q. Li, C. He, Y. Liu, T. Huang, G. Liu, B. Zheng, H. Yang *et al.*, Absence of near-ambient superconductivity in LuH<sub>2±x</sub>N<sub>y</sub>, *Nature (London)* **620**, 72 (2023).
- [33] Y. Zhang, X. Ming, Q. Li, X. Zhu, B. Zheng, Y. Liu, C. He, H. Yang, and H. Wen, Pressure induced color change and evolution of metallic behavior in nitrogen-doped lutetium hydride, *Sci. China Phys. Mech. Astron.* **66**, 287411 (2023).
- [34] X. Xing, C. Wang, L. Yu, J. Xu, C. Zhang, M. Zhang, S. Huang, X. Zhang, B. Yang, X. Chen *et al.*, Observation of non-superconducting phase changes in LuH<sub>2±x</sub>N<sub>y</sub>, *Nat. Commun.* **14**, 5991 (2023).
- [35] N. P. Salke, A. C. Mark, M. Ahart, and R. J. Hemley, Evidence for near ambient superconductivity in the Lu-N-H system, [arXiv:2306.06301](https://arxiv.org/abs/2306.06301).
- [36] R. Lucrezi, P. P. Ferreira, M. Aichhorn, and C. Heil, Temperature and quantum anharmonic lattice effects in lutetium trihydride: Stability and superconductivity, [arXiv:2304.06685](https://arxiv.org/abs/2304.06685).
- [37] D. Dorde, P. Garcia-Goiricelaya, Y. Fang, J. Ibañez-Azpiroz, and I. Errea, *Ab initio* study of the structural, vibrational and optical properties of potential parent structures of nitrogen-doped lutetium hydride, *Phys. Rev. B* **108**, 064517 (2023).
- [38] P. P. Ferreira, L. J. Conway, A. Cucciari, S. D. Cataldo, F. Giannessi, E. Kogler, L. T. F. Eleno, C. J. Pickard, C. Heil, and L. Boeri, Search for ambient superconductivity in the Lu-N-H system, *Nat. Commun.* **14**, 5367 (2023).
- [39] M. Liu, X. Liu, J. Li, J. Liu, Y. Sun, X. Chen, and P. Liu, Parent structures of near-ambient nitrogen-doped lutetium hydride superconductor, *Phys. Rev. B* **108**, L020102 (2023).
- [40] M. Gubler, M. Krummenacher, J. A. Finkler, and S. Goedecker, Ternary phase diagram of nitrogen doped lutetium hydrides, [arXiv:2306.07746](https://arxiv.org/abs/2306.07746).
- [41] F. Xie, T. Lu, Z. Yu, Y. Wang, Z. Wang, S. Meng, and M. Liu, Lu-H-N phase diagram from first-principles calculations, *Chin. Phys. Lett.* **40**, 057401 (2023).
- [42] K. P. Hilleke, X. Wang, D. Luo, N. Geng, B. Wang, and E. Zurek, Structure, stability and superconductivity of N-doped lutetium hydrides at kbar pressures, *Phys. Rev. B* **108**, 014511 (2023).
- [43] Z. Huo, D. Duan, T. Ma, Z. Zhang, Q. Jiang, D. An, H. Song, F. Tian, and T. Cui, First-principles study on the conventional superconductivity of N-doped fcc-LuH<sub>3</sub>, *Matter Radiat. Extremes* **8**, 038402 (2023).
- [44] N. S. Pavlov, I. R. Shein, K. S. Pervakov, V. M. Pudalov, and I. A. Nekrasov, Anatomy of the band structure of the newest apparent near-ambient superconductor LuH<sub>3-x</sub>N<sub>x</sub>, *JETP Lett.* (2023).
- [45] A. Denchfield, H. Park, and R. J. Hemley, Novel electronic structure of nitrogen-doped lutetium hydrides, [arXiv:2305.18196](https://arxiv.org/abs/2305.18196).
- [46] Y. Sun, F. Zhang, S. Wu, V. Antropov, and K. Ho, Effect of nitrogen doping and pressure on the stability of LuH<sub>3</sub>, *Phys. Rev. B* **108**, L020101 (2023).
- [47] W. Wu, Z. Zeng, and X. Wang, Investigations of pressurized Lu-N-H materials by using the hybrid functional, *J. Phys. Chem. C* **127**, 20121 (2023).
- [48] G. Kresse and J. Furthmüller, Efficient iterative schemes for *ab initio* total-energy calculations using a plane-wave basis set, *Phys. Rev. B* **54**, 11169 (1996).
- [49] J. P. Perdew, J. A. Chevary, S. H. Vosko, K. A. Jackson, M. R. Pederson, D. J. Singh, and C. Fiolhais, Atoms, molecules, solids, and surfaces: Applications of the generalized gradient approximation for exchange and correlation, *Phys. Rev. B* **46**, 6671 (1992).
- [50] P. E. Blöchl, Projector augmented-wave method, *Phys. Rev. B* **50**, 17953 (1994).
- [51] J. Heyd, G. E. Scuseria, and M. Ernzerhof, Hybrid functionals based on a screened Coulomb potential, *J. Chem. Phys.* **118**, 8207 (2003).
- [52] S. L. Dudarev, G. A. Botton, S. Y. Savrasov, C. J. Humphreys, and A. P. Sutton, Electron-energy-loss spectra and the structural stability of nickel oxide: An LSDA+*U* study, *Phys. Rev. B* **57**, 1505 (1998).
- [53] M. Cococcioni and S. D. Gironcoli, Linear response approach to the calculation of the effective interaction parameters in the LDA+*U* method, *Phys. Rev. B* **71**, 035105 (2005).
- [54] See Supplemental Material at <http://link.aps.org/supplemental/10.1103/PhysRevResearch.5.043238> for the lattice parameters of *Fm-3m* LuH<sub>3</sub> as a function of pressure compared with DFT calculations, DFT+*U* calculations, and experimental data; crystal structures of Lu-N-H hydrides; enthalpy curves per formula unit as a function of pressure for LuH<sub>3</sub> and Lu<sub>12</sub>H<sub>35</sub>N; the phonon dispersion relations for LuH<sub>3</sub> and ternary Lu-N-H hydrides at different pressures; the dependence of minimum dynamically stable pressure on N-doping concentration; the simulated XRD patterns of Lu-N-H hydrides, LuN and Lu<sub>2</sub>O<sub>3</sub>; calculated electronic band structure of *Fm-3m* LuH<sub>3</sub> using PBE and HSE hybrid functional at 60 GPa; calculated electronic band structures of *Fm-3m* LuH<sub>3</sub> and *Pm-3m* Lu<sub>4</sub>H<sub>11</sub>N with and without SOC at 60 GPa; electronic DOS of ternary Lu-N-H hydrides at 60 GPa; the dependence of DOS value at the Fermi level on N-doping concentration; superconductivity of *Fm-3m* LuH<sub>3</sub> at 24 and 120 GPa; dependence of *T<sub>c</sub>*'s on N-doping concentration in LuH<sub>3</sub> and Lu-N-H superconductors; the number of different structures when a nitrogen atom replaces a hydrogen atom in any position for different supercell sizes of *Fm-3m* LuH<sub>3</sub>; the lattice parameters and unit cell volume of *Fm-3m* LuH<sub>3</sub> and *Pm-3m* Lu<sub>4</sub>H<sub>11</sub>N at 60 GPa; detailed structural information of ternary Lu-N-H hydrides. The Supplemental Material also contains Refs. [27,28,38,42–43,55].
- [55] T. Palasyuk and M. Tkacz, Pressure-induced structural phase transition in rare-earth trihydrides. Part I. (GdH<sub>3</sub>, HoH<sub>3</sub>, LuH<sub>3</sub>), *Solid State Commun.* **133**, 481 (2005).
- [56] C. Su, J. Lv, Q. Li, H. Wang, L. Zhang, Y. Wang, and Y. Ma, Construction of crystal structure prototype database: Methods and applications, *J. Phys.: Condens. Matter* **29**, 165901 (2017).
- [57] A. Togo, F. Oba, and I. Tanaka, First-principles calculations of the ferroelastic transition between rutile-type and CaCl<sub>2</sub>-type SiO<sub>2</sub> at high pressures, *Phys. Rev. B* **78**, 134106 (2008).
- [58] P. Giannozzi, S. Baroni, N. Bonini, M. Calandra, R. Car, C. Cavazzoni, D. Ceresoli, G. L. Chiarotti, M. Cococcioni, I. Dabo *et al.*, QUANTUM ESPRESSO: A modular and open-source

- software project for quantum simulations of materials, *J. Phys.: Condens. Matter* **21**, 395502 (2009).
- [59] C. J. Pickard and R. J. Needs, Structure of phase III of solid hydrogen, *Nat. Phys.* **3**, 473 (2007).
- [60] A. Meninno and I. Errea, *Ab initio* study of metastable occupation of tetrahedral sites in palladium hydrides and its impact on superconductivity, *Phys. Rev. B* **107**, 024504 (2023).
- [61] I. Errea, M. Calandra, C. J. Pickard, J. R. Nelson, R. J. Needs, Y. Li, H. Liu, Y. Zhang, Y. Ma, and F. Mauri, Quantum hydrogen-bond symmetrization in the superconducting hydrogen sulfide system, *Nature (London)* **532**, 81 (2016).
- [62] F. Belli and I. Errea, Impact of ionic quantum fluctuations on the thermodynamic stability and superconductivity of  $\text{LaBH}_8$ , *Phys. Rev. B* **106**, 134509 (2022).
- [63] I. Errea, F. Belli, L. Monacelli, A. Sanna, T. Koretsune, T. Tadano, R. Bianco, M. Calandra, R. Arita, F. Mauri *et al.*, Quantum crystal structure in the 250-kelvin superconducting lanthanum hydride, *Nature (London)* **578**, 66 (2020).
- [64] G. Gao, R. Hoffmann, N. W. Ashcroft, H. Liu, A. Bergara, and Y. Ma, Theoretical study of the ground-state structures and properties of niobium hydrides under pressure, *Phys. Rev. B* **88**, 184104 (2013).
- [65] Y. Wei, J. Yuan, F. I. Khan, G. Ji, Z. Gu, and D. Wei, Pressure induced superconductivity and electronic structure properties of scandium hydrides using first principles calculations, *RSC Adv.* **6**, 81534 (2016).
- [66] P. B. Allen and R. C. Dynes, Transition temperature of strong-coupled superconductors reanalyzed, *Phys. Rev. B* **12**, 905 (1975).